Nontypeable *Haemophilus influenzae* infection impedes *Pseduomonas aeruginosa* colonization and persistence in mouse respiratory tract

Natalie Lindgren [1,2], Lea Novak[3], Benjamin C. Hunt [1,2], Melissa S. McDaniel [1,2], and W. Edward Swords [1,2#]

[1] Department of Medicine, Division of Pulmonary, Allergy, and Critical Care Medicine

[2] Gregory Fleming James Center for Cystic Fibrosis Research

[3] Department of Pathology, Division of Anatomic Pathology

University of Alabama at Birmingham

Running title: Competitive infections in CF related opportunists

Key words: Cystic fibrosis, bacteria, *Haemophilus*, *Pseudomonas*, biofilm

Communicating author:

1918 University Boulevard, MCLM 818

Birmingham, AL 35294

wswords@uabmc.edu

ABSTRACT

Patients with cystic fibrosis (CF) experience lifelong respiratory infections which are a significant cause of morbidity and mortality. These infections are polymicrobial in nature wherein the predominant bacterial species changes as patients age. Young patients have populations dominated by pathobionts such as nontypeable *Haemophilus influenzae* (NTHi), that are eventually supplanted by pathogens such as *Pseudomonas aeruginosa* (*Pa*), which are more typical of late-stage CF disease. In this study, we investigated how initial colonization with NTHi impacts colonization and persistence of *Pa* in the respiratory tract. Analysis of polymicrobial biofilms *in vitro* by confocal microscopy revealed that NTHi promoted greater levels of *Pa* biofilm volume and diffusion. However, sequential infection of mice with NTHi followed by *Pa* showed significant reduction in *Pa* in the lungs as compared to infection with *Pa* alone. Coinfected mice also had reduced severity of airway tissue damage and lower levels of inflammatory cytokines as compared mice infected with *Pa* alone. Similar results were observed using heat-inactivated NTHi bacteria prior to *Pa* introduction. Based on these results, we conclude that NTHi can significantly reduce susceptibility to subsequent *Pa* infection, most likely due to immune priming rather than a direct competitive interaction between species. These findings have potential significance with regard to therapeutic management of early life infections in patients with CF.

Word count: 214 words

INTRODUCTION

Cystic fibrosis (CF) is an autosomal recessive genetic illness that causes dysfunctional ionic transport at epithelial surfaces, with concomitant impacts on mucociliary defenses and clearance in the lungs. As a consequence, patients with CF experience lifelong infections of the airway mucosa that cause chronic inflammation and epithelial damage, among other sequelae (1-3). Despite therapeutic gains that have significantly increased average lifespan for CF patients, airway infections and associated respiratory complications remain a leading cause of morbidity and mortality in patients with CF disease (4). The microbial populations within the CF lung are complex, polymicrobial communities that undergo dynamic changes that correlate with patients' age and overall health, and can be a determinant of disease severity (3, 5-7). Despite years of study of opportunistic infections in the context of CF, there remains much to be learned about how specific pathogens and opportunists impact the course and severity of disease (6-9). Nontypeable *Haemophilus influenzae* (NTHi) is a non-encapsulated, Gram-negative pathobiont that normally resides in the human nasopharynx and upper airways as part of the normal flora. (10-12). Although typically benign in healthy individuals, NTHi is among the most common bacterial species isolated from CF patients during the first year of life and is thus thought of as a common early-stage pathogen (13-15). As with other mucosal airway infections, NTHi persists in the lung within biofilm communities (16, 17).

As CF patients age, the bacterial population diversity typically declines, and patients become chronically colonized with late-stage pathogens such as *Pseudomonas aeruginosa* (*Pa*) (8, 9, 18, 19). *Pa* is a Gram-negative opportunistic pathogen that has a high level of inherent resistance to antimicrobials and host immune effectors and is therefore difficult to treat (20). To adapt to the CF airway environment, *Pa* populations typically undergo a genetic conversion to a mucoid phenotype that overexpresses the exopolysaccharide alginate, which is a component of *Pa* biofilm (21, 22). Mucoid conversion of *Pa* is associated with increased antibiotic resistance, persistent inflammation, and overall worse clinical outcomes (23). Initial *Pa* infections, which

may take place within the first year of life, frequently become chronic after mucoid conversion (19, 20). While the role of *Pa* in end-stage CF disease has been well established, less has been done to establish the role of *Pa* in early-stage CF disease, particularly the ages in which NTHi colonization peaks in frequency (4, 9). We hypothesize that the NTHi infections that are common in early childhood in CF, can potentially influence subsequent infections, with impacts on progression of CF disease.

Bacteria reside in the CF lung as a complex, evolving polymicrobial community in which individual organisms may interact with one another in a synergistic, antagonistic, or null fashion (11, 24-26). Changes in these communities as different species, or strains within species, interact are thought to greatly influence antibiotic susceptibility, immune evasion, and mutations for chronic colonization, all influencing patient outcomes (8, 27). In order to better model the polymicrobial airway infections associated with CF and other conditions, we have carried out multispecies experimental approaches (5, 8, 28). While we know that *Pa* and NTHi clearly reside in the airways at the same time, there is still a need for better understanding of how each species is impacted during polymicrobial infection.

RESULTS

In this study, we aimed to assess the polymicrobial interaction between NTHi and *Pa* both *in vitro* and *in vivo*, using clinically isolated bacterial strains from patients with CF. Mice were intratracheally infected with NTHi and/or mucoid *Pa* (mPA) to produce localized, acute respiratory infections. To model the temporal acquisition of NTHi and *Pa* in CF patients, we tested whether pre-colonization with NTHi influences colonization of *Pa* and began to characterize how this interaction may influence the innate immune response.

Nontypeable *H. influenzae* and *P. aeruginosa* form polymicrobial biofilms *in vitro* that support *Pa* growth.

In any environment that contains more than one bacterial species, including the CF lungs, organisms may interact with one another synergistically, competitively, or null (5)(6). To begin to characterize the polymicrobial interaction between NTHi and *Pa*, we first wanted to evaluate how these two organisms form a polymicrobial biofilm *in vitro*. Since NTHi and *Pa* are typically acquired sequentially over a patient's lifespan, dual-species static biofilms were sequentially seeded with NTHi 86028NP-gfp+, followed by mPA 08-31-mCherry+ 12 hours later. Polymicrobial biofilms were grown for a total of 18 hours, while single-species biofilms of NTHi and *Pa* were grown for 12 hours and 6 hours, respectively, at 37°C + 5% CO_2. These timepoints for growth were selected based on the peak viability of NTHi and *Pa*, as determined by counts of viability over time (Fig. S1A in supplemental material). Due to limitations of differential plating that do not allow for quantification of both organisms in an NTHi/*Pa* co-culture, viable colony counts of *Pa* from sequential dual biofilms were compared to single-species *Pa* biofilms only to assess how pre-introduction of NTHi may influence *Pa* growth. *In vitro*, it appears that pre-colonization with NTHi has no significant impact on *Pa* growth when both organisms are inoculated at roughly the same amount (~10^8 CFU/mL) (Fig. S1B).

We then visualized NTHi 86028NP-gfp+ and mPA 08-31-mCherry+ single- and dual-species fluorescent biofilms with confocal laser scanning microscopy (CLSM) after 18 hours of growth. In single-species biofilms, both organisms formed lawn structures with some towers (Fig. 1A and B). Sequentially seeded dual-species biofilms showed a complex lawn with more diffuse *Pa* colony formation that appeared to support *Pa* growth. As expected, the spatial orientation of dual biofilms were stratified, reflecting the sequential introduction of NTHi followed by *Pa*, with a significant lawn structure of NTHi on the bottom (Fig. 1C). Quantification of *Pa* in both single- and dual-species biofilms by BiofilmQ software revealed that the total volume of *Pa* biofilm is greater in dual-species biofilms than in single-species *Pa* biofilms (Fig. 2A). Segmentation within BiofilmQ software allowed for fluorescent images to be divided by 1 μm cubes with each cube being individually tracked. Following segmentation, the mean cube surface is calculated as the number of points between occupied and unoccupied volume in cube. The calculated mean cube surface showed that dual biofilms have more *Pa* than single-species *Pa* biofilms, recapitulating the results seen with total biofilm volume and verifying the accuracy of cubing (Fig. 2B). This segmentation technique was used for further 3D visualization of single- and dual-species biofilms of *Pa.* Segmentation shows that there is more diffuse local density of *Pa* associated with dual-species (Fig. 2C) rather than single-species (Fig. 2D) growth. Overall, this quantification suggests that *in vitro*, NTHi may positively influence *Pa* growth, producing greater biofilm volume and more dispersed spatial distribution when grown together compared to a single-species *Pa* biofilm.

Nontypeable *H. influenzae* infection decreases bacterial burden of *P. aeruginosa* in mouse lung

While our *in vitro* results suggest that NTHi and *Pa* may positively interact in polymicrobial biofilms, we aimed to evaluate how each species is impacted during polymicrobial infection within the host. Through serial passage, we induced antibiotic resistance in a CF sputum-

derived clinical isolate of NTHi, HI-1, developing a model strain for acute infection (NTHi HI-1r) that can be differentially plated in the presence of *Pa*. To model the sequential acquisition of an early life pathogen (NTHi) followed by a later-stage pathogen (*Pa*) that typically ensues as CF patients age, BALB/cJ mice were intratracheally infected with NTHi HI-1r (inoculum ~10^8 CFU/mouse) followed by a mucoid *P. aeruginosa* isolate, mPA 08-31 (inoculum ~10^7 CFU/mouse) 24 hours later. Both organisms colonized the lungs and were detectable by viable plate counting of lung homogenate 48 hours post-infection. However, colonization of *Pa* was significantly impeded after sequential introduction with NTHi compared to a *Pa* single-infection (**P<0.01) (Fig. 3A). To determine the importance of temporal spacing in this interaction, we also infected mice with both organisms concurrently (inoculum ~10^7 CFU/mL of each). When we compared the bacterial burden of *Pa* in the lungs after a single-infection, a sequential dual-infection, and a concurrent dual-infection, we saw that mice sequentially infected with NTHi followed by *Pa* showed significant reduction in *Pa* abundance compared to a *Pa* only infection (*P<0.05). Additionally, sequential dual-infection resulted in less *Pa* in lung homogenate than concurrent dual-infection (****P<0.0001) (Fig. 3B). This suggests that the competitive interaction between NTHi and *Pa* is dependent on time of introduction and *Pa* abundance in the lungs is only impeded during sequential infection. Histopathological analysis of hematoxylin and eosin (H&E) stained lung sections indicated immune cell infiltration and inflammation 48 hours after infection of both NTHi and *Pa* infection. (Fig. 3C). H&E stained slides were graded for severity of lung injury as indicated by neutrophil infiltration of alveoli, peri-vascular inflammation and peri-bronchial inflammation. At 48-hours post-infection, where a high burden of both NTHi and *Pa* were present in the airways, there was moderate tissue damage for all infection groups with no difference between groups. All infections resulted in significantly more severe tissue damage than a PBS control infection (****P<0.0001) (Fig. 3D). Immune cell infiltration was expressed by total cell infiltrates counted in the bronchoalveolar lavage fluid (BALF) after cytospin preparation and differential staining. As expected from histological results, all infection groups showed

significantly elevated total cell counts, as well as PMN infiltrates in those counts, than uninfected controls with no significant difference between infection groups (*P<0.05, **P<0.01, ***P<0.001, ****P<0.0001) (Fig. 3E-F). Weight loss per animal was evaluated over the course of infection and weight loss increased compared to uninfected controls (Fig. S2A). Taken together, these results suggests that *in vivo*, NTHi impedes the bacterial burden of *Pa* in the airways when introduced sequentially, but not concurrently, and infection with either organism results in respiratory tissue damage with significant inflammatory response.

Impacts of nontypeable *H. influenzae* on *P. aeruginosa* are not strain-specific.

Our coinfection results indicate that a clinical isolate of NTHi, HI-1r, significantly inhibits the bacterial burden of mucoid *P. aeruginosa* isolate mPA 08-31 in the airways. To determine if the impact of NTHi on *Pa in vivo* is strain specific, we induced antibiotic resistance in laboratory strain NTHi 86-028NP to develop strain NTHi 86r, allowing for differential plating of NTHi and *Pa*. Following the sequential infection schematic previously described, we intratracheally introduced NTHi 86-028NPr (inoculum ~10^8 CFU/mouse) into the airways of BALBc/J mice followed by introduction of mPA 08-31 (inoculum ~10^7 CFU/mouse) 24 hours later. Unlike the positive interaction between NTHi and *Pa* seen in our polymicrobial biofilms with the parent strain of NTHi 86r (NTHi 86-028NP), in the airways, viable colony counts of *Pa* were significantly decreased after pre-introduction with NTHi 86r compared to a *Pa* single-infection (*P<0.05) (Fig. 4A). Mucoid conversion of *Pa* is a common consequence of long-term colonization (19, 24, 29). For most patients, the initial colonizing *Pa* strain is nonmucoid, and can remain so for relatively long periods of persistent infection (19). To extend the impact of this phenotype to patients colonized with *Pa* before and after mucoid conversion, we then determined if NTHi pre-introduction impedes the abundance of non-mucoid *Pa.* To do this, we performed sequential infections with the clinical NTHi HI-1r followed by a non-mucoid *Pa* (PA FRD1*mucA+).* Viable colony counts from lung homogenate revealed that, as in preceding

infection studies, *Pa* counts were significantly diminished after infection with NTHi compared to *Pa* alone (*P<0.05) (Fig. 4B). Weight loss per animal was evaluated over the course of infection and weight loss increased compared to uninfected controls (Fig. S2B-C). These results show that NTHi infection significantly reduces the colonization/persistence of *Pa*, regardless of the specific strain of NTHi or the mucoidy status of *Pa*.

Infection with nontypeable *H. influenzae* followed by *P. aeruginosa* results in less severe airway tissue damage and less inflammatory cytokine infiltration than *P. aeruginosa* alone.

While clinical isolate NTHi Hi-1r persists longer than previously established NTHi strains, such as NTHi 86-028NP (data not shown), this strain still begins to be cleared from the airways of mice around 72 hours post-infection, with viable colony counts below the limit of detection for some animals. We wanted to test if *Pa* abundance is inhibited in the lungs once NTHi clearance begins. BALBc/J mice were intratracheally infected with NTHi HI-1r, followed by mPA 08-31 24 hours later and viable colony counts from lung homogenate were assessed after 72 hours post-dual infection, extending the previously established 48 hour timepoint. As expected, sequential introduction of NTHi prior to *Pa* significantly reduced colonization of *Pa* compared to a *Pa* alone (***P<0.001) (Fig. 5A). Reflecting the inhibition of *Pa* abundance in viable colony counts during dual-infection, histological grading of tissue damage revealed a significantly decreased damage score in dual-infected animals compared to a *Pa* single-infection (**P<0.01) (Fig. 5B). H&E staining of lung sections of each infection group revealed more severe immune cell infiltration, pleuritis, perivascular inflammation, and peri-bronchial inflammation 72 hours post-infection than was seen at the 48 hour post-infection timepoint (Fig. 5C). Finally, total cell counts in BALF and the percentage of PMN infiltrates in those counts was not different among single or dual-infection groups, but was significantly increased compared to uninfected controls (*P<0.05,

**P<0.01, ****P<0.0001) (Fig. 5D-E). Weight loss per animal was evaluated over the course of infection and weight loss increased compared to uninfected controls (Fig. S2D).

To evaluate the host immune response following NTHi and *Pa* single or dual-infections, we measured cytokine and chemokine levels in BALF with DuoSet ELISA kits designed to detect inflammatory markers including MCP-1, TNF-α, IL-10, IL-1α, IL-1β, or IL-6. Several of these well-established inflammatory markers, including MCP-1, TNF-α, and the anti-inflammatory marker IL-10 were significantly higher after *Pa* single-infection compared to a dual-infection with both NTHi and *Pa* (****P<0.0001). (Fig. 6A-C). While IL-1α, IL-1β and IL-6 levels were not different between single and dual-infected groups at 72 hours post-infection, the temporal regulation of these acute response markers indicate that they may be associated with earlier timepoints after bacterial introduction (Fig. 6D-F). Taken together, these data suggest that at 72 hours post-infection, after bacterial clearance has begun, NTHi still inhibits *Pa* bacterial burden in the lungs. In addition to impeding abundace of *Pa*, sequential infection reduces the severity of damage to airway tissues, as measured by histological scoring, and reduces inflammatory cytokine levels in BALF.

Inhibitory effect of nontypeable *H. influenzae* on *P. aeruginosa* infection is independent of bacterial viability.

Previous polymicrobial studies suggest that NTHi may impact subsequent infections directly via interspecies interaction, or by priming the host response (30-33). To determine if the impact of preceding infection on *Pa* requires viable NTHi bacteria, we sequentially infected mice with heat-killed NTHi HI-1r (HK NTHi HI-1r) (inoculum equvialent to ~10^8 CFU/mL) followed by mucoid *P. aeruginosa* mPA 08-31 (inoculum ~10^7 CFU/mL) for 48 hours. The total infection time of this experiment was 72 hours, repeating our previously established timepoint in which live NTHi infection reduced *Pa* infection. Viable colony counts from lung homogenate showed *Pa*

counts were still significantly reduced by pre-treatment with heat-killed NTHi (*P<0.05) (Fig. 7A). Additionally, *Pa* infection resulted in a significantly higher histolopathological score than HK NTHi/*Pa* dual-infection, suggesting that non-viable NTHi is sufficient to protect the lung parenchyma from the severe effects of *Pa* infection, indicating the protection from tissue damage previously seen at this time point during dual-infection is independent of NTHi viability (**P<0.01) (Fig. 7B). H&E stained lung sections harvested from this experiment showed more neutrophilic infiltration and more severe tissue damage after *Pa* single-infection compared to dual-infection (Fig. 7C). As previously seen, the total cell counts in BALF and the percentage of PMN infiltration was not different among single or dual-infection groups, but was significantly increased compared to uninfected controls (*P<0.05, ***P<0.001, ****P<0.0001) (Fig. 5D-E). Overall, we found that heat-killed NTHi is sufficient to significantly impede the abundance of *Pa* in the lungs at 72 hours post-infection, suggesting that the interaction between NTHi and *Pa* may be entirely mediated by the immune response of the host.

DISCUSSION

With the advent and widespread use of culture independent technologies for profiling microbial consortia, it has become clear that the populations within the lungs of patients with CF are diverse and subject to dynamic change. These shifts are likely of importance in determining whether species will persist or be cleared, as well as in the initiation of the inflammatory events that are a hallmark of CF disease (6-8, 24, 34, 35). The consequences of respiratory exacerbations include an intense neutrophilic inflammatory response that can cause significant lung damage and decreased respiratory function, contributing significantly to the morbidity and mortality associated with CF disease (8, 35). There is still much to learn regarding how specific organisms interact within the compromised respiratory tract of CF airways and how these interactions influence disease progression (8).

The complex microbial communities in the lung often change in dominant species and overall population diversity as patients age (19, 24). Decreased microbial diversity and the emergence of mucoid *Pa* as the dominant microbial species are significantly associated with detrimental host immune response, lung functional decline, and eventual patient mortality (19, 24). Previous studies have focused on characterizing key CF pathogens individually, however, these infections are undoubtedly polymicrobial in nature, influencing the pathogenesis of disease as organisms interact (3, 19). Nontypeable *Haemophilus influenzae*, a typically benign colonizer of nasopharyngeal region in healthy individuals, has long been recognized as an opportunistic pathogen of the airway mucosa, including in young children with CF (10, 36). While it is clear that NTHi and *Pa* share a common niche within the CF lung, including patients with coinfections, there remains much to be learned regarding how these organisms influence one another (14, 26-27). Our work considers the interaction between and disease consequences of two key CF pathogens, NTHi, as early-life pathogen, and *Pa*, a late-stage pathogen that can be acquired early in life.

Polymicrobial interactions in static biofilms provide basic information about interspecies bacterial interactions. Our results indicate that NTHi and *Pa* form polymicrobial biofilms that may support *Pa* growth (Fig. 1-2). However, to understand polymicrobial infections in patients, we must how these two organisms interact within the lung environment. In a mouse model, we tested how NTHi impacted *Pa* abundance in the lungs following sequential introduction, representing how patients typically acquire these organisms over time, contrasted with concurrent acquisition. We found that both NTHi and *Pa* colonize and persist in murine lungs for at least 48 hours in single-infections, but viable colony counts of *Pa* from lung homogenate were significantly reduced only following sequential introduction with NTHi (Fig. 3). This competitive inhibition contrasts with the cooperative interaction seen in dual-species biofilms, possibly because of the additional factor of the host immune response.

Bacterial infections in the CF lungs result in chronic inflammation as microbial and phagocytic debris buildup in the airways, contributing to the reduced lung function and overactive immune response associated with exacerbations (12). The inherently diminished airways defenses associated with CFTR dysfunction are thought to predispose CF patients to frequent microbial infections followed by an inadequate, yet overactive, innate immune response that further initiate tissue damage by airway remodeling (12, 29). Histopathological analysis of lung sections can evaluate immune cell infiltration within alveoli, pleura, perivascular and peri-bronchial spaces, and grade the severity of tissue damage. In CF, the ensuing tissue damage following chronic bacterial infection is a strong indicator of respiratory failure, the leading cause of morbidity and mortality (14). Pre-introduction with NTHi not only reduces the bacterial burden of *Pa* in the lungs, but also significantly reduces the visible epithelial damage compared to a *Pa* single-infection, an effect that may reduce detrimental airway remodeling following infection (Fig. 5). While dual-infection reduces the severity of airway parenchymal damage, we wanted to know if inflammatory cytokine levels were reduced after dual-infection as well. The BALF collected from single- and dual-infected mice showed trending decreases in

early response cytokines, such as IL-1-α, IL-1-β, and IL-6 in dual-infected mice compared to a *Pa* single-infection (Fig. 6A-C). Since the interleukins are some of the first cytokines to respond to bacterial stimuli, we suspect that significant differences between dual- and single-infected groups may appear at earlier timepoints, prior to 72 hours post-infection (13, 30). We saw a significant decrease in inflammatory cytokine levels of MCP-1, TNF-α, and IL-10 in sequentially infected duals compared to a *Pa* single-infection, suggesting that the reduction in bacterial burden also diminishes a potentially harmful innate immune response (Fig. 6D-F). Most notably, this reduction in TNF-α could extend beneficial effects for CF patients, as the continual production of this early response cytokine indicates an ongoing and overactive innate immune response in the CF lungs (13).

While we suspect that NTHi and *Pa* are interacting in vivo, understanding the mechanism of their interaction would provide a valuable therapeutic target. Previous studies have noted that NTHi is capable of interacting with other bacterial species via interspecies quorum signaling, a form of interbacterial communication that can influence the establishment of polymicrobial biofilms and the development of chronic infection. This mechanism of interaction commonly utilizes highly conserved interspecies signaling molecules that facilitate communication across species, commonly through a canonical signal, autoinducer-2 (16). Alternatively, NTHi has also been known to participate in a host-pathogen interactions that overtly exclude the successful colonization of other pathogens, allowing for niche competition by activation of opsonophagocytic killing (17). Therefore, possible mechanisms of interaction between NTHi and *Pa* could be broadly categorized as active, requiring live bacterial cells, or passive, solely reliant on cellular components. To determine if NTHi and *Pa* are engaging in a pathogen-pathogen or host-pathogen interaction, we sequentially infected animals with heat-killed NTHi HI-1r, followed by *Pa* 24 hours later. The introduction of heat-inactivated bacterial components of NTHi provided the pathogen-associated-molecular-patterns (PAMPs) necessary to mount an innate immune response against NTHi components, broadly including the

lipooligosaccharide (LOS) and other protein components, prior to *Pa* introduction (13). We found that even in the absence of live bacteria, pre-introduction of NTHi is capable of diminishing *Pa* bacterial burden in the lungs (Fig. 7A). This indicates that the host inflammatory response is key to *Pa* bacterial clearance, suggesting the interaction between NTHi and *Pa* is host-pathogen mediated. It is also important to note that our infection studies were carried out in mice with normal CFTR function; extending these studies into genetically altered CF mutant animals will be an important avenue for future work.

Defining how different microbes interact within the CF lung to impact bacterial colonization, persistence, and host response has the potential to guide rational treatment strategies to lengthen periods of asymptomatic or mildly symptomatic infection that are typically associated with younger patients. The results of our infection studies indicate that colonization of the lung with NTHi may provide inherent resistance to subsequent colonization with *Pa*. A likely mechanism for such an effect would be stimulation of innate immune defenses, which can prime host phagocyte responses to respond to incoming pathogens (31, 33, 37, 38). These results raise interesting possibilities regarding whether aggressive treatment against early-stage opportunists, such as NTHi, may be contraindicated or even harmful by providing a susceptibility window to other infections. It is also notable that for opportunistic airway infections associated with COPD, an extensive body of recent work indicates that treatment with inflammatory agonists that evoke innate responses can confer protection and are under active investigation as therapeutics (39-43). The concept of therapeutically inducing a low level of airway inflammation to enhance resistance may merit further study in CF related infections.

MATERIALS AND METHODS

Bacterial strains and growth conditions

NTHi 86-028NP is well characterized patient isolate for which a fully annotated genome sequence data base is available (44). NTHi HI-1 is a sputum-derived isolate from a pediatric patient with CF and was provided by Timothy Starner (University of Iowa Children's Hospital). NTHi 86-028NPr and NTHi HI-1r were derived from NTHi 86-028NP and NTHi HI-1 by serial passage on plates containing spectinomycin (18). NTHi 86-028NP-gfp+ was constructed by electroporation with plasmid PGM1.1+gfp (provided by K. Mason, Nationwide Childrens' Research Hospital) (45, 46). For heat-killed NTHi experiments, bacteria were scraped from a plate into sterile PBS, resuspended to ~10^9 CFU/ml, and incubated at 65°C for 1 h; bacterial killing was confirmed by lack of growth. All NTHi strains were routinely cultured on supplemented brain-heart infusion (sBHI) agar (Difco), containing 10 µg/mL of hemin (ICN Biochemical) and 1µg/mL of NAD (Sigma).

P. aeruginosa mPA08-31 is a mucoid clinical isolate from a CF patient at UAB Hospital, and was provided by S. Birket (University of Alabama at Birmingham) (47, 48). *A* nonmucoid derivative of *P. aeruginosa*, (*P. aeruginosa* FRD1*mucA*+) was provided by J. Scoffield (University of Alabama at Birmingham) (49). *P. aeruginosa* mPA08-31-mCherry+ was derived by electroporation with plasmid pUCP19+mCherry (provided by D. Wozniak, Ohio State University). All *P. aeruginosa* strains were routinely cultured on Luria-Bertani (LB) agar (Difco). Strains were streaked for colony isolation before inoculation into LB broth and shaking overnight at 37°C and 200 rpm.

Confocal microscopy of static biofilms

In vitro biofilms were prepared by resuspending NTHi 86028NP-gfp+ from an overnight plate culture to~10^8 CFU/ml in 2x sBHI, or overnight broth culture of mPA08-31-mCherry+ diluted to ~10^8 CFU/ml in LB broth. Dual-species biofilms were sequentially seeded with NTHi 86028NP-

gfp+ preceding mPA08-31-mCherry+ by 12 hours into a 35-mm glass-bottom confocal dish (MatTek) in 2-ml increments such that the final density in each well was ~10^8 CFU of one or of both organisms. NTHi 86028NP-gfp+ single-species biofilms grew for 12 hours. mPA08-31-mCherry+ single-species biofilms grew for 6 hours. Sequentially seeded dual biofilms grew for 18 hours. All dishes were incubated at 37°C with 5% CO_2 before being washed with sterile PBS and fixed with 4% paraformaldehyde (Alfa Aesar, Tewksbury, MA). Viable colony counts of mPA08-31-mCherry+ from single and dual-species biofilms were obtained by plating on LB (antibiotic selection). Confocal laser scanning microscopy (CLSM) was performed using a Nikon-A1R HD25 confocal laser microscope (Nikon, Tokyo, Japan) at the University of Alabama at Birmingham. All images were processed using the NIS-elements 5.0 software.

Fluorescent biofilm quantification

Fluorescent biofilms were quantified using BiofilmQ software (50). Single fluorescence channels were automatically segmented using the Otsu algorithm. Background was removed with semi-manually thresholding denoising. Global biofilm parameters of the fluorescence channel representing *Pa* were quantified for both single-species and dual-species biofilms to assess biovolume. 3D spatial representation of cubing (representing 1 μm per cube) was calculated by BiofilmQ and visualized with ParaView according to manufacturer's instructions.

Mouse model of respiratory infections

BALB/cJ mice (8 to 10 weeks old) were obtained from Jackson Laboratories (Bar Harbor, ME). For single-species infections, mice were anesthetized with isoflurane and intratracheally infected with NTHi (~10^9 CFU in 100 μl PBS) or *Pa* (~10^8 CFU in 100 μL PBS). For dual infections, mice were anesthetized with isoflurane and infected intratracheally either concurrently with NTHi and *Pa* (~10^9 CFU NTHi and ~10^8 CFU *Pa* in 100 μL PBS), or sequentially, in which infection with NTHi occurred 24 hours prior to *Pa* introduction. For viable

plate counting, the left lung of each mouse was harvested and homogenized in 500 µL of sterile PBS at 30 Hz/s. Lung homogenate was serially diluted in PBS and plated LB agar to obtain viable colony counts of *Pa* and sBHI agar containing spectinomycin (2 mg/mL) for selection of NTHi HI-1r. All samples from polymicrobial infections were also plated on sBHI without antibiotic for total bacterial counts of both organisms. For histological analysis, the right lung of each animal was inflated with 10% buffered formalin and stored at 4°C until processing. All mouse infection protocols were approved by the University of Alabama at Birmingham (UAB) Institutional Animal Care and Use Committees.

Bronchoalveolar lavage fluid collection

Bronchoalveolar lavage was performed by flushing lungs with 6 ml of cold PBS in 1-mL increments as previously described (19). Collected BALF was stored on ice until processing and the first 1mL isolated was centrifuged (1350 × *g*, 5 min) to separate the supernatant from immune cells. The cell pellet was used for total and differential cell counts. The remaining 5 mL of collected BALF was stored at -20°C until use for cytokine analyses.

Cytokine analyses and differential cell counting

Cytokine analyses were performed on the 5 mL of collected BALF via DuoSet ELISA kits (R&D Systems, Minnesota, MN). For total and differential cell counts, cell pellets from BALF were resuspended in fresh PBS and mounted on a slide by cytospin at 500 rpm for 5 minutes. Cells were stained with a Kwik-Diff differential cell stain (ThermoFisher Scientific, Waltham, MA). Three representative fields from each spot were counted to determine the composition of immune cells.

Histological analysis

Inflated right lungs from infected animals were stored in 10% neutral buffered formalin (Fisher Scientific, Waltham, MA) at 4°C until processing. Sections from each lobe of the right lung were trimmed and sent to the UAB Comparative Pathology Laboratory to be paraffin embedded, sectioned and stained with hematoxylin and eosin (H&E). Images of lung sections (200 x magnification) were taken with Olympus DP25 camera (Tokyo, Japan) using an Olympus BX40 microscope. Semiquantitative grading of all lung sections was performed by a board-certified surgical pathologist (L.N.). Semiquantitative histopathological scores were assigned using a scoring matrix based primarily on neutrophilic influx. Severity was rated on a scale of 0 to 3, where 0 represents no observable neutrophils,1 represents dispersed acute inflammation (mild damage), 2 represents dense infiltration (moderate damage), and 3 represents solid infiltrate with necrosis (severe damage). of the section affected of independently viewed fields of view. The final histopathological score represents the maximum grade assigned to each replicate.

Statistical analyses

All bar graphs represent sample means ± standard error of the mean (SEM). All mouse experiments were repeated at least two times and data from independent experiments were combined for analyses. For nonparametric analyses, differences between groups were analyzed by Kruskal-Wallis test with the uncorrected Dunn's test for multiple comparisons. For normally distributed data sets, as determined by Shapiro-Wilk normality test, a one-way analysis of variance (ANOVA) was used with Tukey's multiple-comparison test. Outliers were detected via the ROUT method (Q, 1%) and excluded from the analysis. All statistical tests were performed using GraphPad Prism 9 (San Diego, CA).

ACKNOWLEDGMENTS

The authors gratefully acknowledge helpful input and discussions with colleagues in the UAB Center for Cystic Fibrosis Research. This work was supported by grants to W.E.S. from the Cystic Fibrosis Foundation (CFFSWORDS1810 and CFFSWORDS20G0). N.L. was a predoctoral trainee supported by the UAB Cystic Fibrosis Foundation Basic Research Center (Steven Rowe, PI). B.C.H. was supported by a fellowship from the UAB Predoctoral Training Program in Lung Biology (T32 HL13640). We also thank Timothy Starner (University of Iowa Children's Hospital), Daniel Wozniak (Ohio State University), Jessica Scoffield (UAB), and Susan Birket (UAB) for providing the bacterial strains for this study.

Figure Legends

Fig. 1: Nontypeable *H. influenzae* and *P. aeruginosa* form polymicrobial biofilms *in vitro*.

Sequentially seeded biofilms on abiotic surface of A) single-species *P. aeruginosa* mPA 08-31 (pUCP19+mCherry+) B) Nontypeable *H. influenzae* 86-028NP (PGM1.1+gfp) and C) dual-species NTHi and *Pa* in both single channels and merged. Inoculation of NTHi preceded *Pa* by 12 hours and both organisms grew for additional 6 hours at 37 °C + 5% CO_2 (18 hours total). Imaged at 40X magnification. Scale bar represents 50 µm.

Fig. 2 Quantification of nontypeable *H. influenzae* and *P. aeruginosa* polymicrobial biofilms.

Bacterial density within fluorescent biofilms was quantified using BiofilmQ software to measure A) biofilm volume of *Pa* in dual and single-species biofilms and B) mean cube surface of *Pa* quantified as 1 cube = 1µm. Cubing can be visualized as local density of *Pa* in both C) a sequentially seeded dual-species biofilm and D) a single-species *Pa* biofilm. Mean ± SEM. (N = 4). Mann-Whitney test, two-tailed, *P<0.05.

Fig. 3: Nontypeable H. influenzae diminishes *P. aeruginosa* abundance in murine lungs.

BALBc/J mice were intratracheally infected with nontypeable *H. influenzae* (NTHi Hi-1r) either 24 hours prior to introduction of mucoid *P. aeruginosa* (mPA 08-31) in a sequential fashion, or were introduced at the same time (concurrently) and assessed 48 post-infection. A) Bacterial counts of NTHi and *Pa* in the lung homogenate enumerated by viable colony counting. B) Bacterial counts of *Pa* in the lung homogenate comparing sequential and concurrent introduction. Severity of disease was indicated by C) H&E stained lung sections (200x

471 magnification) and D) semi-quantitative grading by a pathologist (L.N.). E) Total cell counts in
472 BALF quantified by differential cell counts. F) Percentage of PMNs in the BALF. Mean ± SEM. (N
473 = 10). LOD = limit of detection. Kruskal-Wallis with Dunn's multiple comparison test, * P<0.05,
474 ** P<0.01, *** P<0.001, **** P<0.0001.

475 **Fig. 4: Nontypeable *H. influenzae* impact on subsequent *P. aeruginosa* infection is strain**
476 **independent.**

477 BALBc/J mice were intratracheally infected with nontypeable *H. influenzae* (NTHi 86r) followed
478 by mucoid *P. aeruginosa* (mPA 08-31). A) Bacterial counts in the lung homogenate were
479 enumerated by viable colony counting 72 hours post- dual infection. Intratracheal infections
480 were also performed with nontypeable *H. influenzae* (NTHi HI-1r) and nonmucoid *P. aeruginosa*
481 (PA FRD1*mucA+)* and B) bacterial counts in the lung homogenate were enumerated by viable
482 colony counting 72 hours post- dual infection. Mean ± SEM. (N = 10). LOD = limit of detection.
483 Kruskal-Wallis with Dunn's multiple comparison test, * P<0.05, ** P<0.01, *** P<0.001, ****
484 P<0.0001.

485 **Fig. 5: Nontypeable *H. influenzae* and *P. aeruginosa* dual-infection reduces the severity of**
486 **airway tissue damage.**

487 BALBc/J mice were intratracheally infected with nontypeable *H. influenzae* (NTHi Hi-1r) 24
488 hours prior to introduction of mucoid *P. aeruginosa* (mPA 08-31) and assessed 72 hours post-
489 dual infection. A) Bacterial counts of NTHi and *Pa* in the lung homogenate enumerated by
490 viable colony counting. (N = 13-15). Severity of disease was indicated by B) semi-quantitative

491 grading by a pathologist (L.N.) and C) H&E stained lung sections (200x magnification) (N = 6-10).
492 D) Total cell counts in BALF quantified by differential counting. (N = 6-8). E) Percentage of PMNs
493 in the BALF (N = 6-9). Mean ± SEM. LOD = limit of detection. Kruskal-Wallis with Dunn's multiple
494 comparison test, * P<0.05, ** P<0.01, *** P<0.001, **** P<0.0001.

495 **Fig. 6: Inflammatory cytokine levels after dual-infection are reduced compared to *P.***
496 ***aeruginosa* infection alone.**

497 Cytokine and chemokine analyses were performed on BALF supernatant from infected or mock-
498 infected mice 72 hours post-infection using a DuoSet ELISA kits for A) MCP-1, B) TNF-α, C) IL-10,
499 D) IL-1α, E) IL-1β, and F) IL-6. Mean ± SEM, (N = 7-10). One-way ANOVA with Tukey's multiple
500 comparisons test for post-hoc analysis. **** P<0.0001.

501 **Fig. 7: Impact of nontypeable *H. influenzae* on *P. aeruginosa* infection is independent of**
502 **bacterial viability.**

503 BALBc/J mice were intratracheally infected with heat-inactivated nontypeable *H. influenzae*
504 (NTHi Hi-1r) 24 hours prior to introduction of mucoid *P. aeruginosa* (mPA 08-31) and assessed
505 72 hours post- dual infection. A) Bacterial counts of NTHi and *Pa* in the lung homogenate were
506 enumerated by viable colony counting. (N = 10). Severity of disease was indicated by B) semi-
507 quantitative grading by a pathologist (L.N.) and C) H&E stained lung sections (200x
508 magnification) (N = 8-10). D) Total cell counts in BALF quantified by differential counting. E)
509 Percentage of PMNs in the BALF. (N = 9-10). Mean ± SEM. LOD = limit of detection. Kruskal-
510 Wallis with Dunn's multiple comparison test, * P<0.05, ** P<0.01, *** P<0.001, **** P<0.0001.

511 **Fig. S1: Quantification of nontypeable *H. influenzae* and *P. aeruginosa* polymicrobial**

512 **fluorescent biofilms.**

513 Viable colony counts of A) single -species NTHI 86-028NP-gfp+ and mPA 08-31-mCherry+ static

514 biofilms seeded at ~10^8 and grown over time. B) Bacterial counts of single- and dual-species

515 static biofilms sequentially seeded at ~10^8 and grown in sBHI broth at 37°C + 5% CO_2 for 18

516 hours total. Dual counts depicts Pa growth. Mean ± SEM. (N = 4-5). Dotted line = inoculum.

517 Kruskal-Wallis with Dunn's multiple comparison test.

518 **Fig. S2: Weight change following nontypeable *H. influenzae* and *P. aeruginosa* infection.**

519 Percentage of initial weight was calculated for all animal infections with weight change

520 compared to uninfected controls. A) Weight change at 48 hours post-infection with NTHi HI-1r

521 and mPA 08-31. B) Weight change at 72 hours post-infection with NTHi 86-028NPr and mPA 08-

522 31. C) Weight change at 72 hours post-infection with NTHi HI-1r and Pa FRD1*mucA+*. D) Weight

523 change at 72 hours post-infection with NTHi HI-1r and mPA 08-31. E) Weigh change at 72 hours

524 post-infection with heat-killed NTHi HI-1r and mPA 08-31. (N = 10-15). Mean ± S1

525

526 SEM. Kruskal-Wallis with Dunn's multiple comparison test, * P<0.05, ** P<0.01, *** P<0.001,

527 **** P<0.0001.

528

529 References:

530 1. Lyczak JB, Cannon CL, Pier GB. 2002. Lung infections associated with cystic fibrosis. Clin
531 Microbiol Rev 15:194-222.

532 2. Ratjen F, Bell SC, Rowe SM, Goss CH, Quittner AL, Bush A. 2015. Cystic fibrosis. Nat Rev
533 Dis Primers 1:15010.

534 3. Magalhaes AP, Lopes SP, Pereira MO. 2016. Insights into Cystic Fibrosis Polymicrobial
535 Consortia: The Role of Species Interactions in Biofilm Development, Phenotype, and
536 Response to In-Use Antibiotics. Front Microbiol 7:2146.

537 4. Foundation CF. 2019. Cystic fibrosis patient registry annual data report.

538 5. O'Toole GA. 2018. Cystic Fibrosis Airway Microbiome: Overturning the Old, Opening the
539 Way for the New. J Bacteriol 200.

540 6. Huang YJ, LiPuma JJ. 2016. The Microbiome in Cystic Fibrosis. Clin Chest Med 37:59-67.

541 7. Caverly LJ, Zhao J, LiPuma JJ. 2015. Cystic fibrosis lung microbiome: opportunities to
542 reconsider management of airway infection. Pediatr Pulmonol 50 Suppl 40:S31-8.

543 8. Filkins LM, O'Toole GA. 2015. Cystic Fibrosis Lung Infections: Polymicrobial, Complex,
544 and Hard to Treat. PLoS Pathog 11:e1005258.

545 9. Zemanick ET, Sagel SD, Harris JK. 2011. The airway microbiome in cystic fibrosis and
546 implications for treatment. Curr Opin Pediatr 23:319-24.

547 10. Erwin AL, Smith AL. 2007. Nontypeable *Haemophilus influenzae*: understanding
548 virulence and commensal behavior. **Trends Microbiol** 15:355-362.

549 11. Dickson RP, Erb-Downward JR, Martinez FJ, Huffnagle GB. 2016. The Microbiome and
550 the Respiratory Tract. Annu Rev Physiol 78:481-504.

551 12. Weinberg F, Dickson RP, Nagrath D, Ramnath N. 2020. The Lung Microbiome: A Central
552 Mediator of Host Inflammation and Metabolism in Lung Cancer Patients? Cancers
553 (Basel) 13.

554 13. Cardines R, Giufre M, Pompilio A, Fiscarelli E, Ricciotti G, Di Bonaventura G, Cerquetti M.
555 2012. Haemophilus influenzae in children with cystic fibrosis: antimicrobial
556 susceptibility, molecular epidemiology, distribution of adhesins and biofilm formation.
557 Int J Med Microbiol 302:45-52.

558 14. Rayner RJ, Hiller EJ, Ispahani P, Baker M. 1990. Haemophilus infection in cystic fibrosis.
559 Arch Dis Child 65:255-8.

560 15. Saliu F, Rizzo G, Bragonzi A, Cariani L, Cirillo DM, Colombo C, Dacco V, Girelli D, Rizzetto
561 S, Sipione B, Cigana C, Lore NI. 2021. Chronic infection by nontypeable Haemophilus
562 influenzae fuels airway inflammation. ERJ Open Res 7.

563 16. Starner TD, Zhang N, Kim G, Apicella MA, McCray PB, Jr. 2006. *Haemophilus influenzae*
564 forms biofilms on airway epithelia: implications in cystic fibrosis. **Am J Respir Crit Care**
565 **Med** 174:213-220.

566 17. Swords WE. 2012. Nontypeable Haemophilus influenzae biofilms: role in chronic airway
567 infections. Front Cell Infect Microbiol 2:97.

568 18. Grahl N, Dolben EL, Filkins LM, Crocker AW, Willger SD, Morrison HG, Sogin ML, Ashare
569 A, Gifford AH, Jacobs NJ, Schwartzman JD, Hogan DA. 2018. Profiling of Bacterial and
570 Fungal Microbial Communities in Cystic Fibrosis Sputum Using RNA. mSphere 3.

571 19. Burns JL, Gibson RL, McNamara S, Yim D, Emerson J, Rosenfeld M, Hiatt P, McCoy K,
572 Castile R, Smith AL, Ramsey BW. 2001. Longitudinal assessment of Pseudomonas
573 aeruginosa in young children with cystic fibrosis. J Infect Dis 183:444-52.

574 20. Gellatly SL, Hancock RE. 2013. Pseudomonas aeruginosa: new insights into pathogenesis
575 and host defenses. Pathog Dis 67:159-73.

576 21. Rossi E, La Rosa R, Bartell JA, Marvig RL, Haagensen JAJ, Sommer LM, Molin S, Johansen
577 HK. 2021. Pseudomonas aeruginosa adaptation and evolution in patients with cystic
578 fibrosis. Nat Rev Microbiol 19:331-342.

579 22. Gill JF, Deretic V, Chakrabarty AM. 1987. Alginate production by the mucoid
580 Pseudomonas aeruginosa associated with cystic fibrosis. Microbiol Sci 4:296-9.

581 23. Mayer-Hamblett N, Aitken ML, Accurso FJ, Kronmal RA, Konstan MW, Burns JL, Sagel SD,
582 Ramsey BW. 2007. Association between pulmonary function and sputum biomarkers in
583 cystic fibrosis. Am J Respir Crit Care Med 175:822-8.

584 24. Burns JL, Emerson J, Stapp JR, Yim DL, Krzewinski J, Louden L, Ramsey BW, Clausen CR.
585 1998. Microbiology of sputum from patients at cystic fibrosis centers in the United
586 States. Clin Infect Dis 27:158-63.

587 25. Dickson RP, Erb-Downward JR, Huffnagle GB. 2013. The role of the bacterial microbiome
588 in lung disease. Expert Rev Respir Med 7:245-57.

589 26. Dickson RP, Erb-Downward JR, Prescott HC, Martinez FJ, Curtis JL, Lama VN, Huffnagle
590 GB. 2014. Cell-associated bacteria in the human lung microbiome. Microbiome 2:28.

591 27. Dickson RP, Huffnagle GB. 2015. The Lung Microbiome: New Principles for Respiratory
592 Bacteriology in Health and Disease. PLoS Pathog 11:e1004923.

593 28. Welp AL, Bomberger JM. 2020. Bacterial Community Interactions During Chronic
594 Respiratory Disease. Front Cell Infect Microbiol 10:213.

595 29. Burns JL, Ramsey BW, Smith AL. 1993. Clinical manifestations and treatment of
596 pulmonary infections in cystic fibrosis. Adv Pediatr Infect Dis 8:53-66.

597 30. Lysenko ES, Clarke TB, Shchepetov M, Ratner AJ, Roper DI, Dowson CG, Weiser JN. 2007.
598 Nod1 signaling overcomes resistance of S. pneumoniae to opsonophagocytic killing.
599 PLoS Pathog 3:e118.

600 31. Lysenko ES, Ratner AJ, Nelson AL, Weiser JN. 2005. The role of innate immune responses
601 in the outcome of interspecies competition for colonization of mucosal surfaces. **PLoS**
602 **Pathog** 1:e1.

603 32. Armbruster CE, Hong W, Pang B, Weimer KE, Juneau RA, Turner J, Swords WE. 2010.
604 Indirect pathogenicity of Haemophilus influenzae and Moraxella catarrhalis in
605 polymicrobial otitis media occurs via interspecies quorum signaling. mBio 1.

606 33. Weimer KE, Armbruster CE, Juneau RA, Hong W, Pang B, Swords WE. 2010. Coinfection
607 with Haemophilus influenzae promotes pneumococcal biofilm formation during
608 experimental otitis media and impedes the progression of pneumococcal disease. J
609 Infect Dis 202:1068-75.

610 34. Hampton TH, Green DM, Cutting GR, Morrison HG, Sogin ML, Gifford AH, Stanton BA,
611 O'Toole GA. 2014. The microbiome in pediatric cystic fibrosis patients: the role of shared
612 environment suggests a window of intervention. Microbiome 2:14.

613 35. Zemanick ET, Harris JK, Wagner BD, Robertson CE, Sagel SD, Stevens MJ, Accurso FJ,
614 Laguna TA. 2013. Inflammation and airway microbiota during cystic fibrosis pulmonary
615 exacerbations. PLoS One 8:e62917.

616 36. Starner TD, McCray PB, Jr., American College of P, American Physiological S. 2005.
617 Pathogenesis of early lung disease in cystic fibrosis: a window of opportunity to
618 eradicate bacteria. Ann Intern Med 143:816-22.

619 37. Ratner AJ, Lysenko ES, Paul MN, Weiser JN. 2005. Synergistic proinflammatory
620 responses induced by polymicrobial colonization of epithelial surfaces. **Proc Natl Acad**
621 **Sci U S A** 102:3429-3434.

622 38. Mukherjee S, Weimer KE, Seok SC, Ray WC, Jayaprakash C, Vieland VJ, Swords WE, Das J.
623 2014. Host-to-host variation of ecological interactions in polymicrobial infections. Phys
624 Biol 12:016003.

625 39. Cleaver JO, You D, Michaud DR, Pruneda FA, Juarez MM, Zhang J, Weill PM, Adachi R,
626 Gong L, Moghaddam SJ, Poynter ME, Tuvim MJ, Evans SE. 2014. Lung epithelial cells are
627 essential effectors of inducible resistance to pneumonia. Mucosal Immunol 7:78-88.

628 40. Duggan JM, You D, Cleaver JO, Larson DT, Garza RJ, Guzman Pruneda FA, Tuvim MJ,
629 Zhang J, Dickey BF, Evans SE. 2011. Synergistic interactions of TLR2/6 and TLR9 induce a
630 high level of resistance to lung infection in mice. J Immunol 186:5916-26.

631 41. Evans SE, Tuvim MJ, Fox CJ, Sachdev N, Gibiansky L, Dickey BF. 2011. Inhaled innate
632 immune ligands to prevent pneumonia. Br J Pharmacol 163:195-206.

633 42. Evans SE, Xu Y, Tuvim MJ, Dickey BF. 2010. Inducible innate resistance of lung
634 epithelium to infection. Annu Rev Physiol 72:413-35.

635 43. Moghaddam SJ, Clement CG, De la Garza MM, Zou X, Travis EL, Young HW, Evans CM,
636 Tuvim MJ, Dickey BF. 2008. Haemophilus influenzae lysate induces aspects of the
637 chronic obstructive pulmonary disease phenotype. Am J Respir Cell Mol Biol 38:629-38.

638 44. Harrison A, Dyer DW, Gillaspy A, Ray WC, Mungur R, Carson MB, Zhong H, Gipson J,
639 Gipson M, Johnson LS, Lewis L, Bakaletz LO, Munson RS, Jr. 2005. Genomic sequence of
640 an otitis media isolate of nontypeable Haemophilus influenzae: comparative study with
641 H. influenzae serotype d, strain KW20. J Bacteriol 187:4627-36.

642 45. Vogel AR, Szelestey BR, Raffel FK, Sharpe SW, Gearinger RL, Justice SS, Mason KM. SapF-
643 mediated heme-iron utilization enhances persistence and coordinates biofilm
644 architecture of Haemophilus. Front Cell Infect Microbiol 2:42.

645 46. Mitchell MA, Skowronek K, Kauc L, Goodgal SH. 1991. Electroporation of *Haemophilus*
646 *influenzae* is effective for transformation of plasmid but not chromosomal DNA. Nucl
647 Acids Res 19:3625-3628.

648 47. Das S, Howlader DR, Zheng Q, Ratnakaram SSK, Whittier SK, Lu T, Keith JD, Picking WD,
649 Birket SE, Picking WL. 2020. Development of a Broadly Protective, Self-Adjuvanting
650 Subunit Vaccine to Prevent Infections by Pseudomonas aeruginosa. Front Immunol
651 11:583008.

652 48. McDaniel MS, Schoeb T, Swords WE. 2020. Cooperativity between Stenotrophomonas
653 maltophilia and Pseudomonas aeruginosa during polymicrobial airway infections. Infect
654 Immun doi:10.1128/IAI.00855-19.

655 49. Silo-Suh LA, Suh SJ, Ohman DE, Wozniak DJ, Pridgeon JW. 2015. Complete Genome
656 Sequence of Pseudomonas aeruginosa Mucoid Strain FRD1, Isolated from a Cystic
657 Fibrosis Patient. Genome Announc 3.

658 50. Hartmann R, Jeckel H, Jelli E, Singh PK, Vaidya S, Bayer M, Rode DKH, Vidakovic L, Diaz-
659 Pascual F, Fong JCN, Dragos A, Lamprecht O, Thoming JG, Netter N, Haussler S, Nadell
660 CD, Sourjik V, Kovacs AT, Yildiz FH, Drescher K. 2021. Quantitative image analysis of
661 microbial communities with BiofilmQ. Nat Microbiol 6:151-156.

662

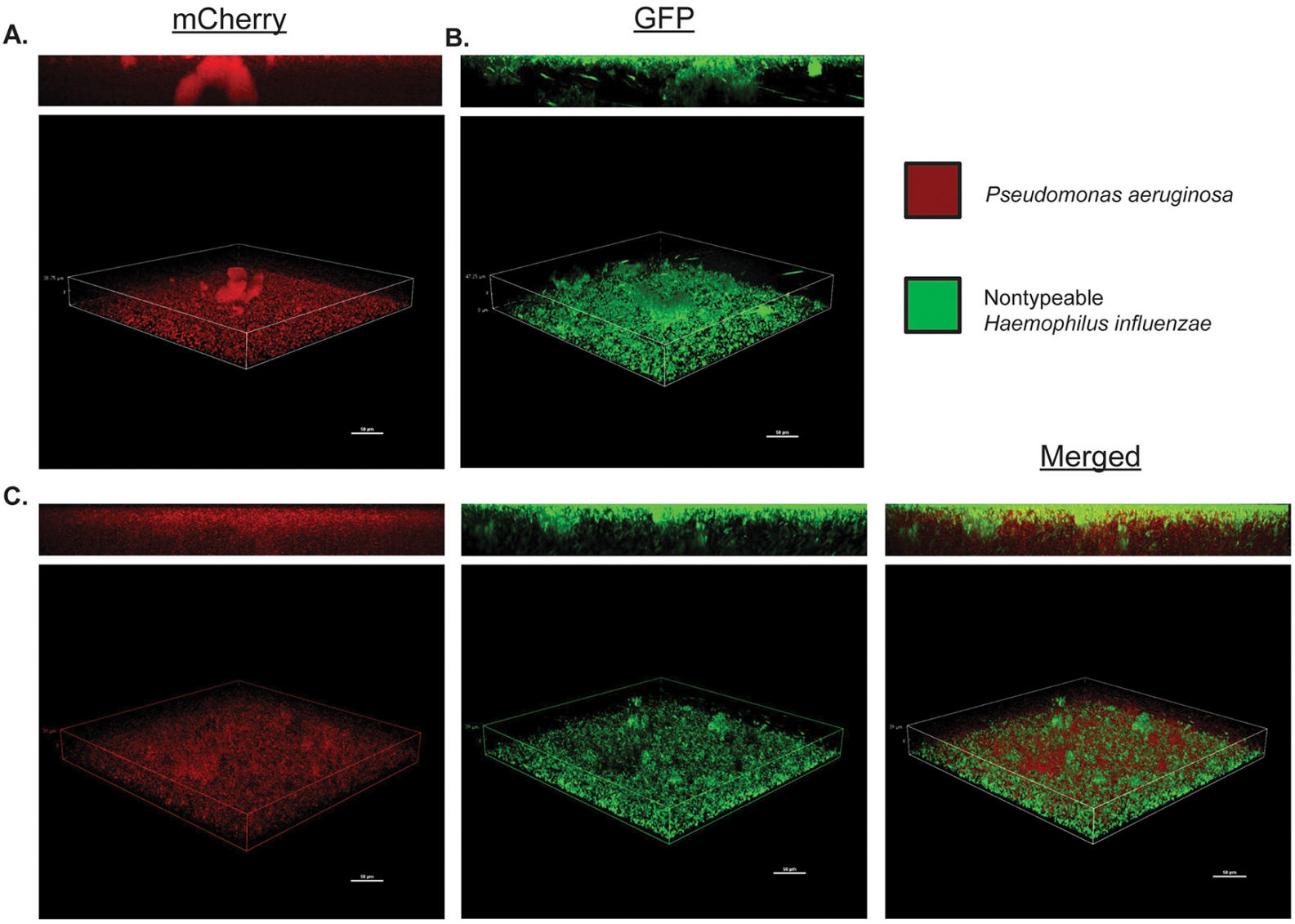

Fig. 1: Nontypeable *H. influenzae* and *P. aeruginosa* form polymicrobial biofilms *in vitro.*
Sequentially seeded biofilms on abiotic surface of A) single-species *P. aeruginosa* mPA 08-31 (pUCP19+mCherry) B) Nontypeable *H. influenzae* 86-028NP (PGM1.1+gfp) and C) dual-species NTHi and *Pa* in both single channels and merged. Inoculation of NTHi preceded *Pa* by 12 hours and both organisms grew for an additional 6 hours at 37 °C + 5% CO_2 (18 hours total). Imaged at 40X magnification. Scale bar represents 50 µm.

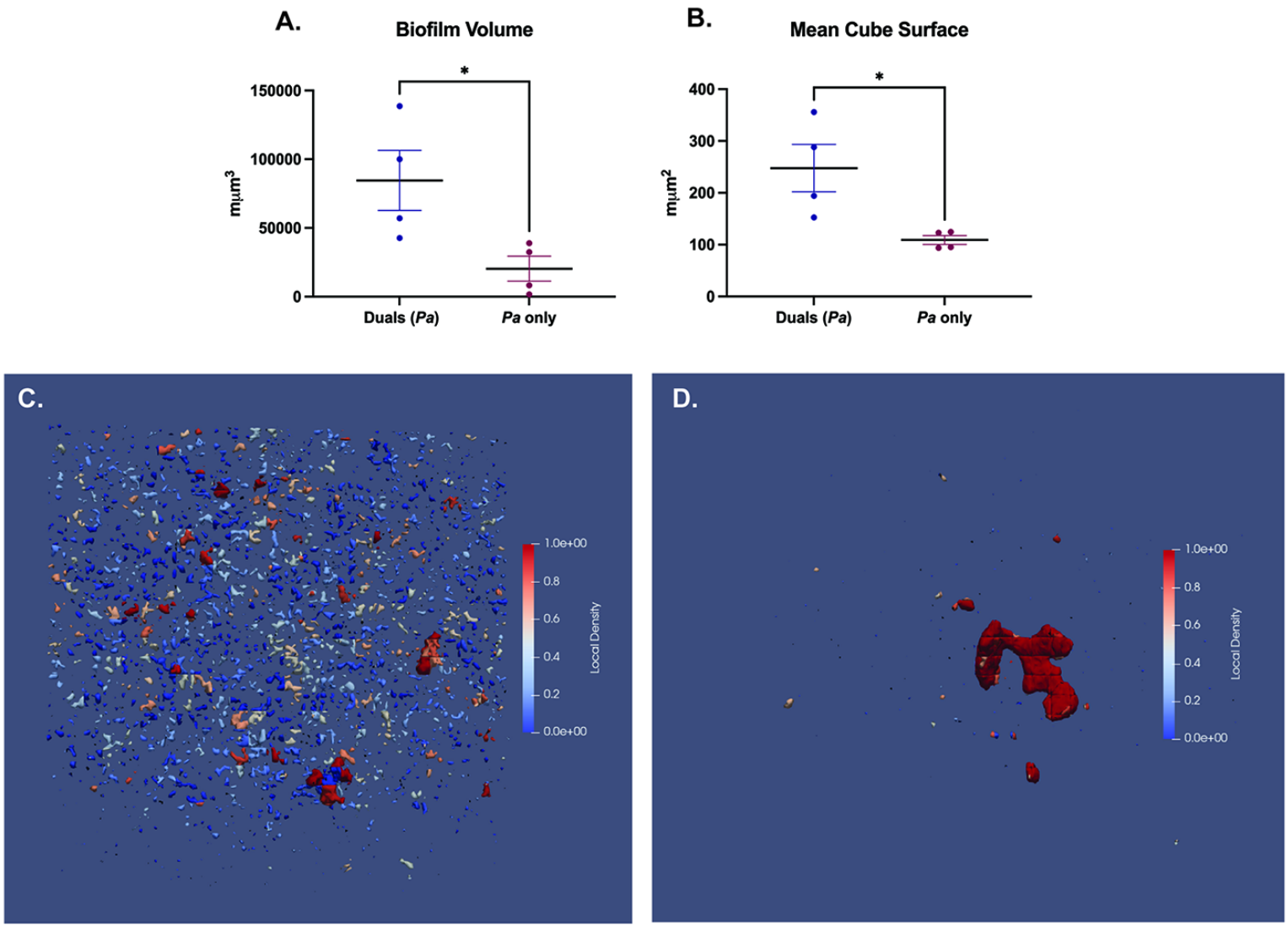

Fig. 2: Quantification of nontypeable *H. influenzae* and *P. aeruginosa* polymicrobial biofilms. Bacterial density within fluorescent biofilms was quantified using BiofilmQ software to measure A) biofilm volume of mPA 08-31(mCherry+) in dual and single-species biofilms and B) mean cube surface of *Pa* quantified as 1 cube = 1μm. Cubing can be visualized as local density of *Pa* in both C) a sequentially seeded dual-species biofilm and D) a single-species *Pa* biofilm. Mean ± SEM. (N = 4). Mann-Whitney test, two-tailed, *P<0.05.

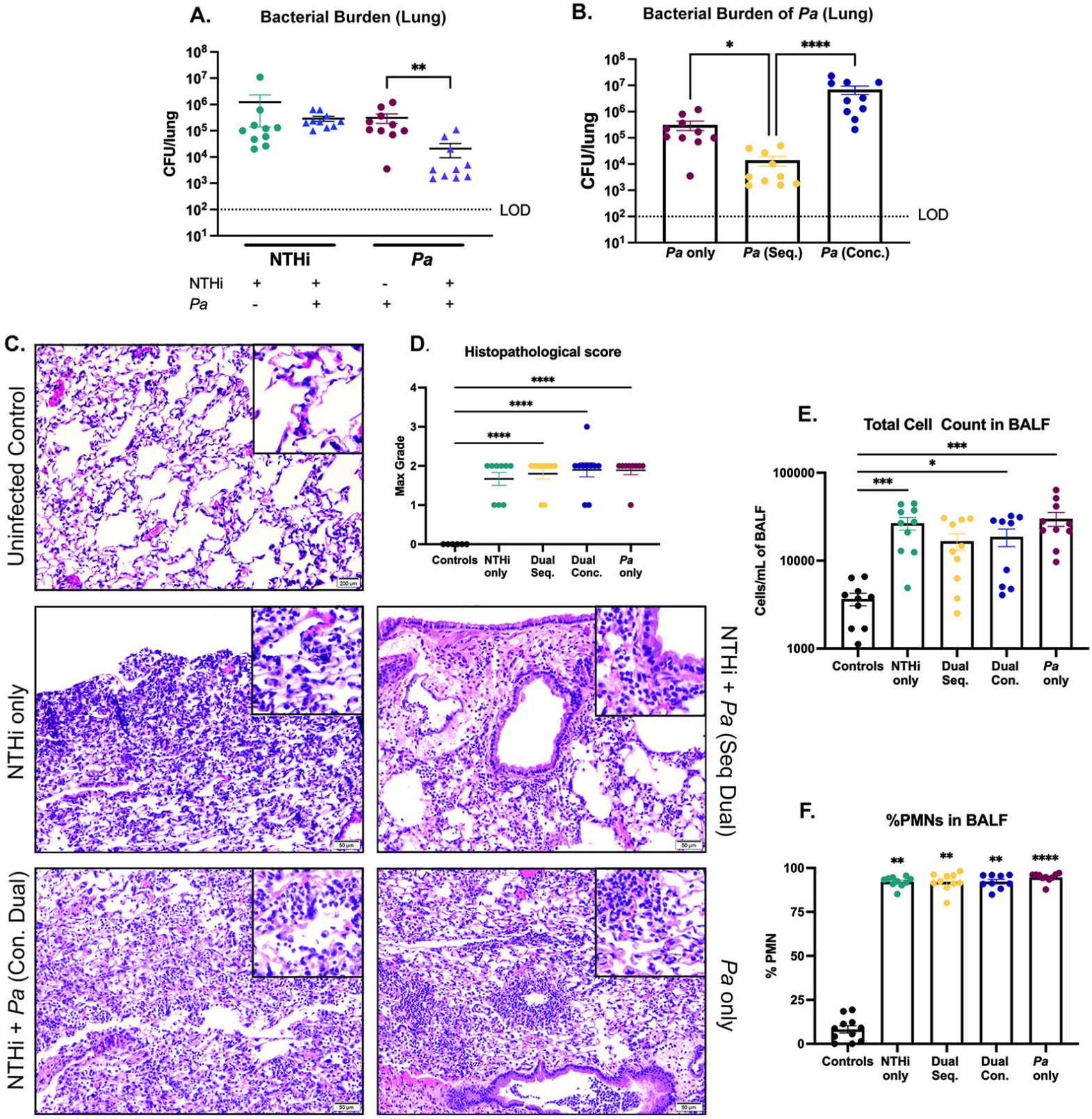

Fig. 3: Nontypeable *H. influenzae* diminishes *P. aeruginosa* abundance in murine lungs. BALBc/J mice were intratracheally infected with nontypeable *H. influenzae* (NTHi Hi-1r) either 24 hours prior to introduction of mucoid *P. aeruginosa* (mPA 08-31) in a sequential fashion, or were introduced at the same time (concurrently) and assessed 48 post-infection. A) Bacterial counts of NTHi and *Pa* in the lung homogenate enumerated by viable colony counting. B) Bacterial counts of *Pa* in the lung homogenate comparing sequential and concurrent introduction. Severity of disease was indicated by C) H&E stained lung sections (200x magnification) and D) semi-quantitative grading by a pathologist (L.N.). E) Total cell counts in BALF quantified by differential cell counts. F) Percentage of PMNs in the BALF. Mean ± SEM. (N = 10). LOD = limit of detection. Kruskal-Wallis with Dunn's multiple comparison test, * P<0.05, ** P<0.01, *** P<0.001, **** P<0.0001.

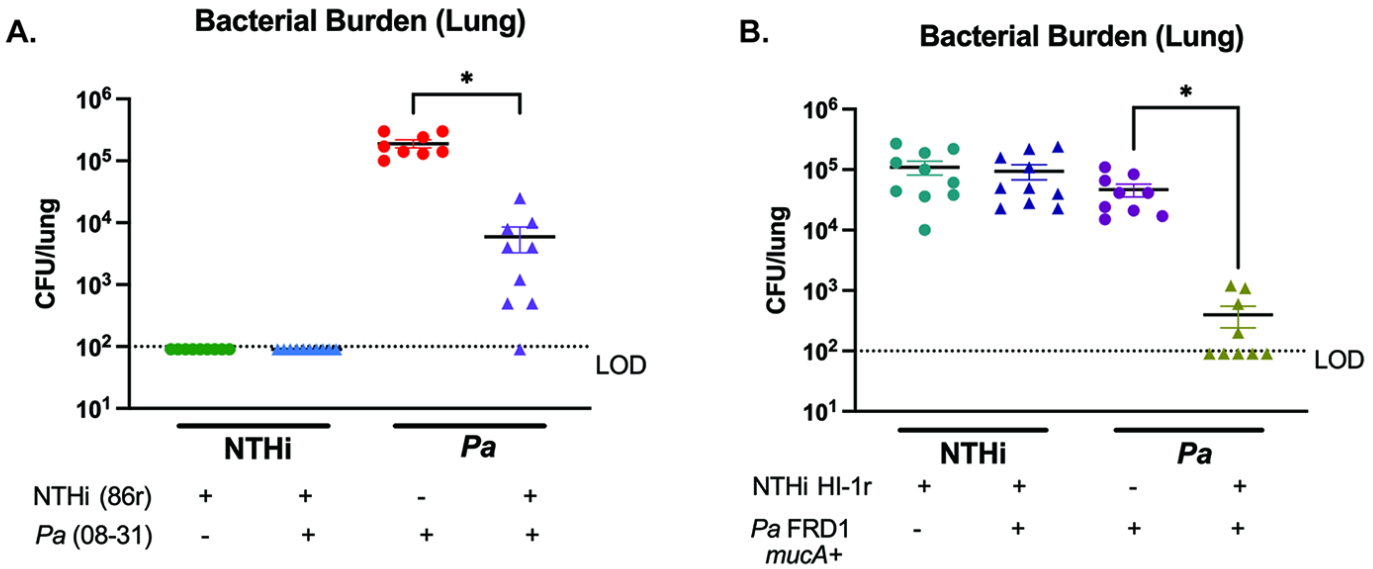

Fig. 4: Nontypeable *H. influenzae* impact on subsequent *P. aeruginosa* infection is strain independent. BALBc/J mice were intratracheally infected with nontypeable *H. influenzae* (NTHi 86r) followed by mucoid *P. aeruginosa* (mPA 08-31). A) Bacterial counts in the lung homogenate were enumerated by viable colony counting 72 hours post- dual infection. Intratracheal infections were also performed with nontypeable *H. influenzae* (NTHi HI-1r) and nonmucoid *P. aeruginosa* (PA FRD1*mucA*+) and B) bacterial counts in the lung homogenate were enumerated by viable colony counting 72 hours post- dual infection. Mean ± SEM. (N = 10). LOD = limit of detection. Kruskal-Wallis with Dunn's multiple comparison test, * P<0.05, ** P<0.01, *** P<0.001, **** P<0.0001.

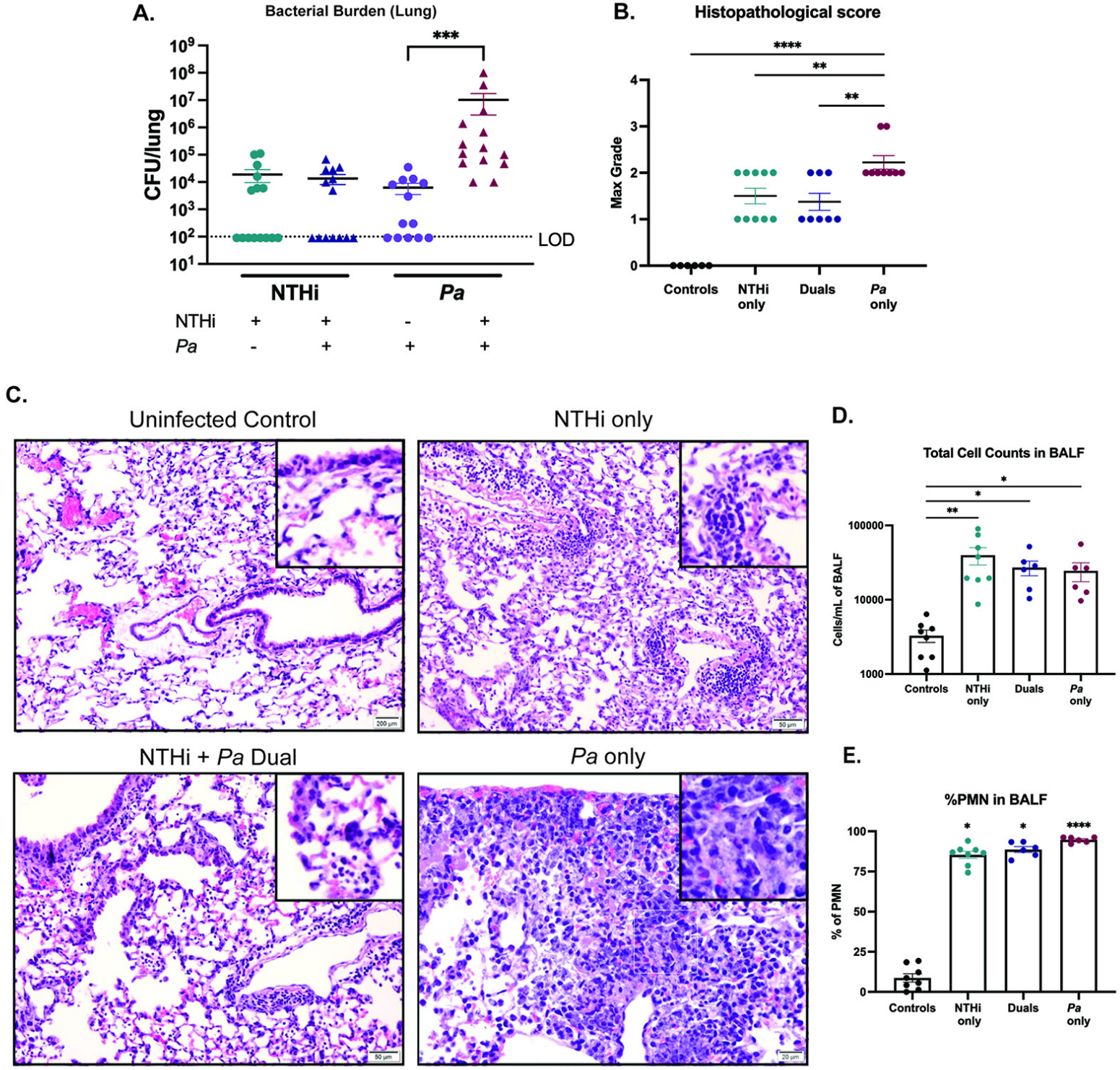

Fig. 5: Nontypeable *H. influenzae* and *P. aeruginosa* dual-infection reduces the severity of airway tissue damage.

BALBc/J mice were intratracheally infected with nontypeable *H. influenzae* (NTHi Hi-1r) 24 hours prior to introduction of mucoid *P. aeruginosa* (mPA 08-31) and assessed 72 hours post- dual infection. A) Bacterial counts of NTHi and *Pa* in the lung homogenate enumerated by viable colony counting. (N = 13-15). Severity of disease was indicated by B) semi-quantitative grading by a pathologist (L.N.) and C) H&E stained lung sections (200x magnification). (N = 6-10). D) Total cell counts in BALF quantified by differential counting. (N = 6-8). E) Percentage of PMNs in the BALF (N = 6-9). Mean ± SEM. LOD = limit of detection. Kruskal-Wallis with Dunn's multiple comparison test, * P<0.05, ** P<0.01, *** P<0.001, **** P<0.0001.

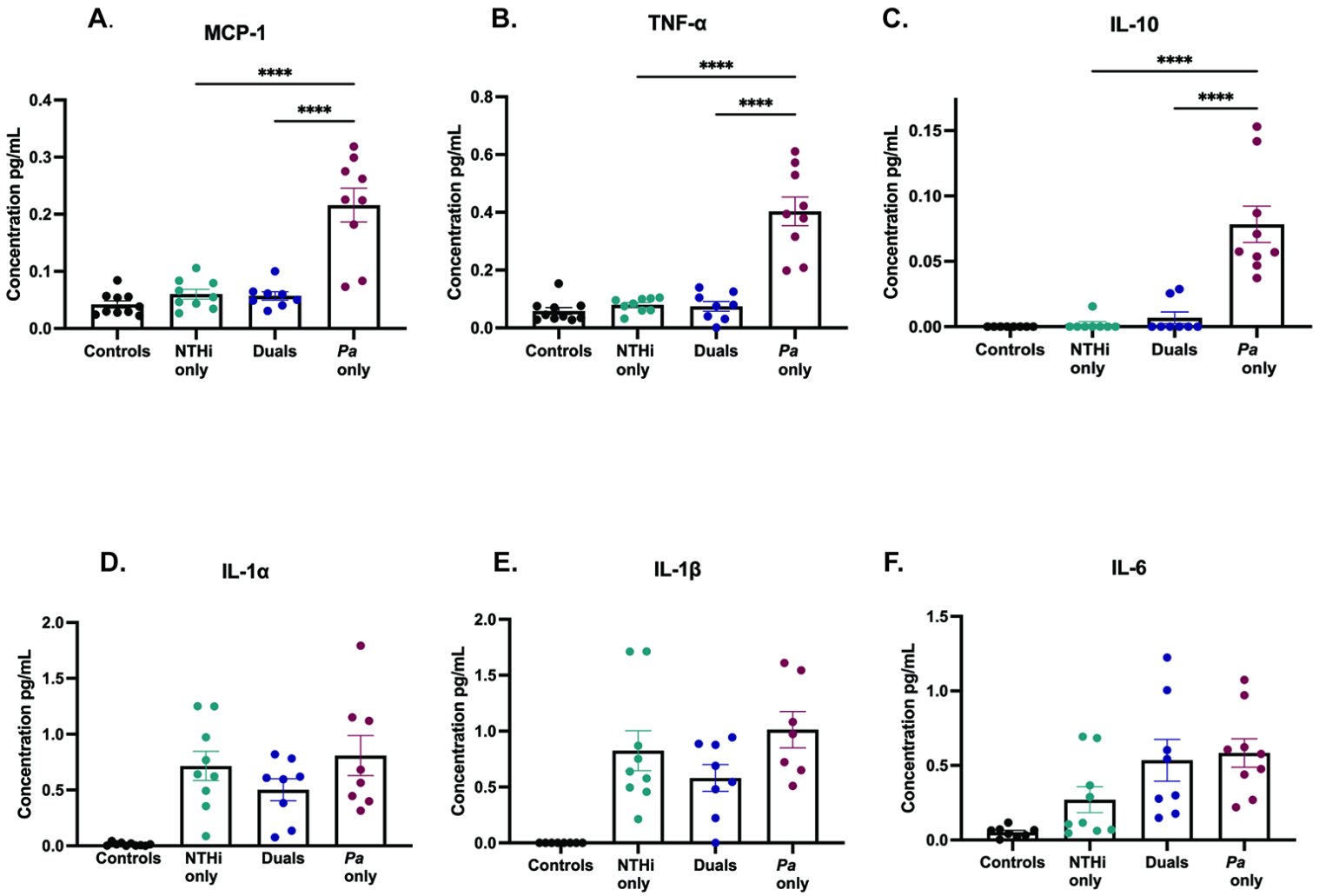

Fig. 6: Inflammatory cytokine levels after dual-infection are decreased compared to *P. aeruginosa* infection alone.

Cytokine and chemokine analyses were performed on BALF supernatant from infected or mock-infected mice 72 hours post-infection using a DuoSet ELISA kits for A) MCP-1, B) TNF-α, C) IL-10, D) IL-1α, E) IL-1β, and F) IL-6 Mean ± SEM, (N = 7-10). One-way ANOVA with Tukey's multiple comparisons test for post-hoc analysis.
**** P<0.0001.

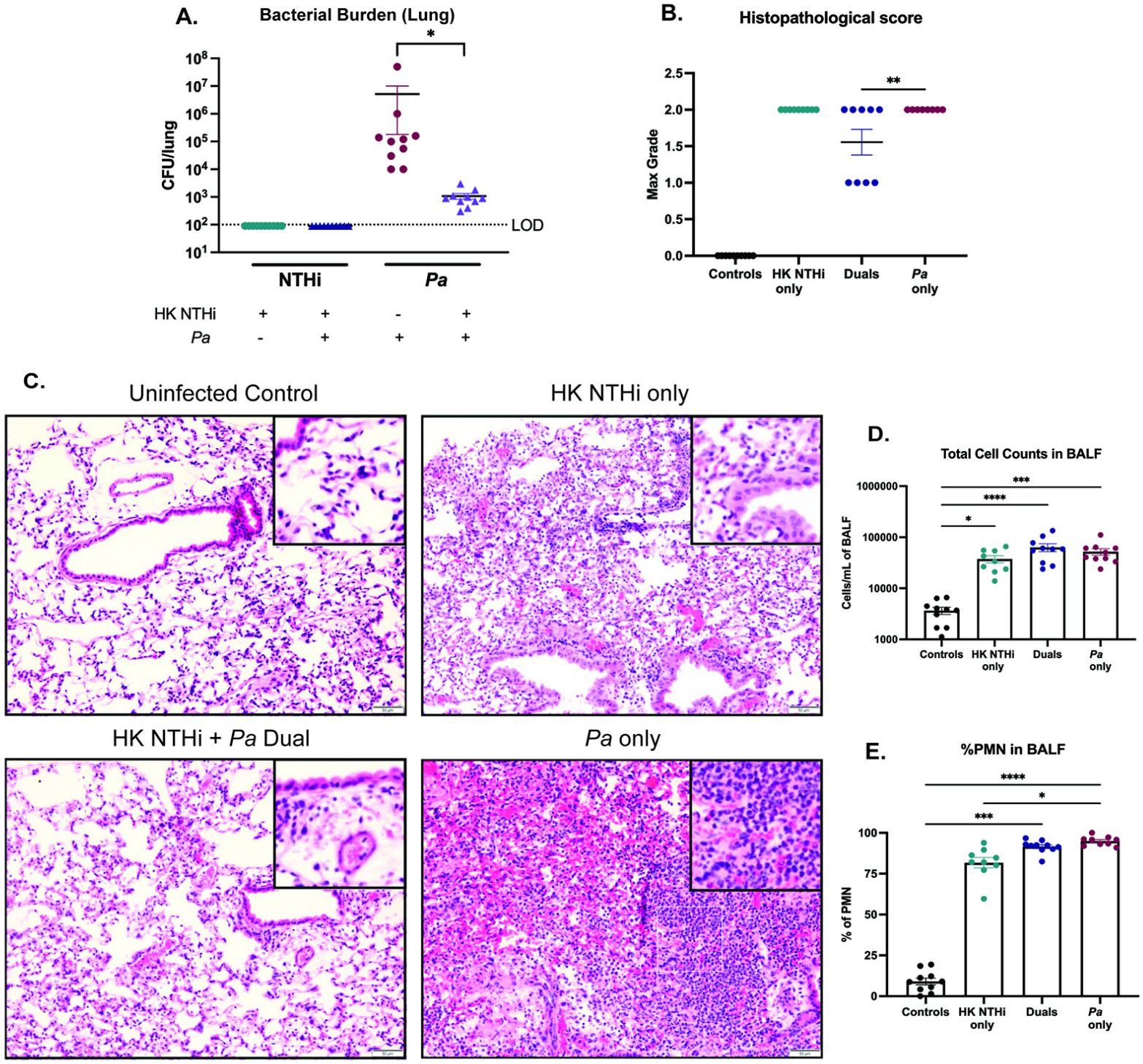

Fig. 7: Impact of nontypeable *H. influenzae* on *P. aeruginosa* infection is independent of bacterial viability. BALBc/J mice were intratracheally infected with heat-inactivated nontypeable *H. influenzae* (NTHi Hi-1r) 24 hours prior to introduction of mucoid *P. aeruginosa* (mPA 08-31) and assessed 72 hours post- dual infection. A) Bacterial counts of NTHi and *Pa* in the lung homogenate were enumerated by viable colony counting. (N = 10). Severity of disease was indicated by B) semi-quantitative grading by a pathologist (L.N.) and C) H&E stained lung sections (200x magnification). (N = 8-10). D) Total cell counts in BALF quantified by differential counting. E) Percentage of PMNs in the BALF. (N = 9-10). Mean ± SEM. LOD = limit of detection. Kruskal-Wallis with Dunn's multiple comparison test, * P<0.05, ** P<0.01, *** P<0.001, **** P<0.0001.

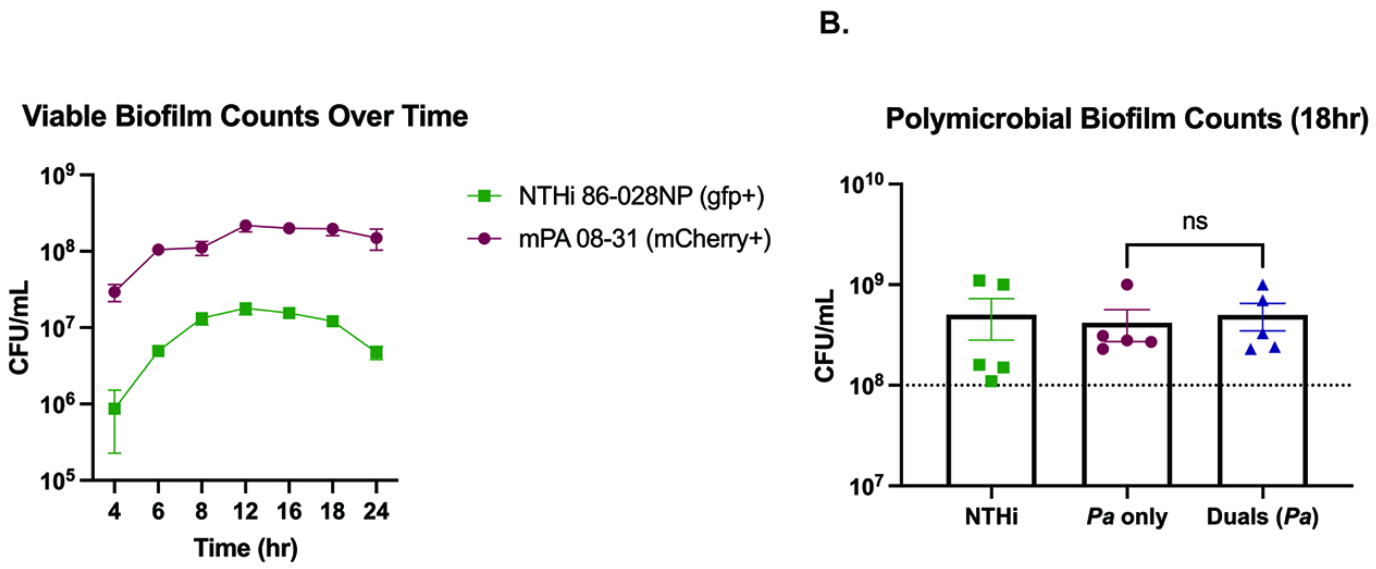

Fig. S1: Quantification of nontypeable *H. influenzae* and *P. aeruginosa* polymicrobial fluorescent biofilms. Viable colony counts of A) single -species NTHI 86-028NP-gfp+ and mPA 08-31-mCherry+ static biofilms seeded at ~10^8 and grown over time. B) Bacterial counts of single- and dual-species static biofilms sequentially seeded at ~10^8 and grown in sBHI broth at 37°C + 5% CO_2 for 18 hours total. Dual counts depicts Pa growth. Mean ± SEM. (N = 4-5). Dotted line = inoculum. Kruskal-Wallis with Dunn's multiple comparison test.

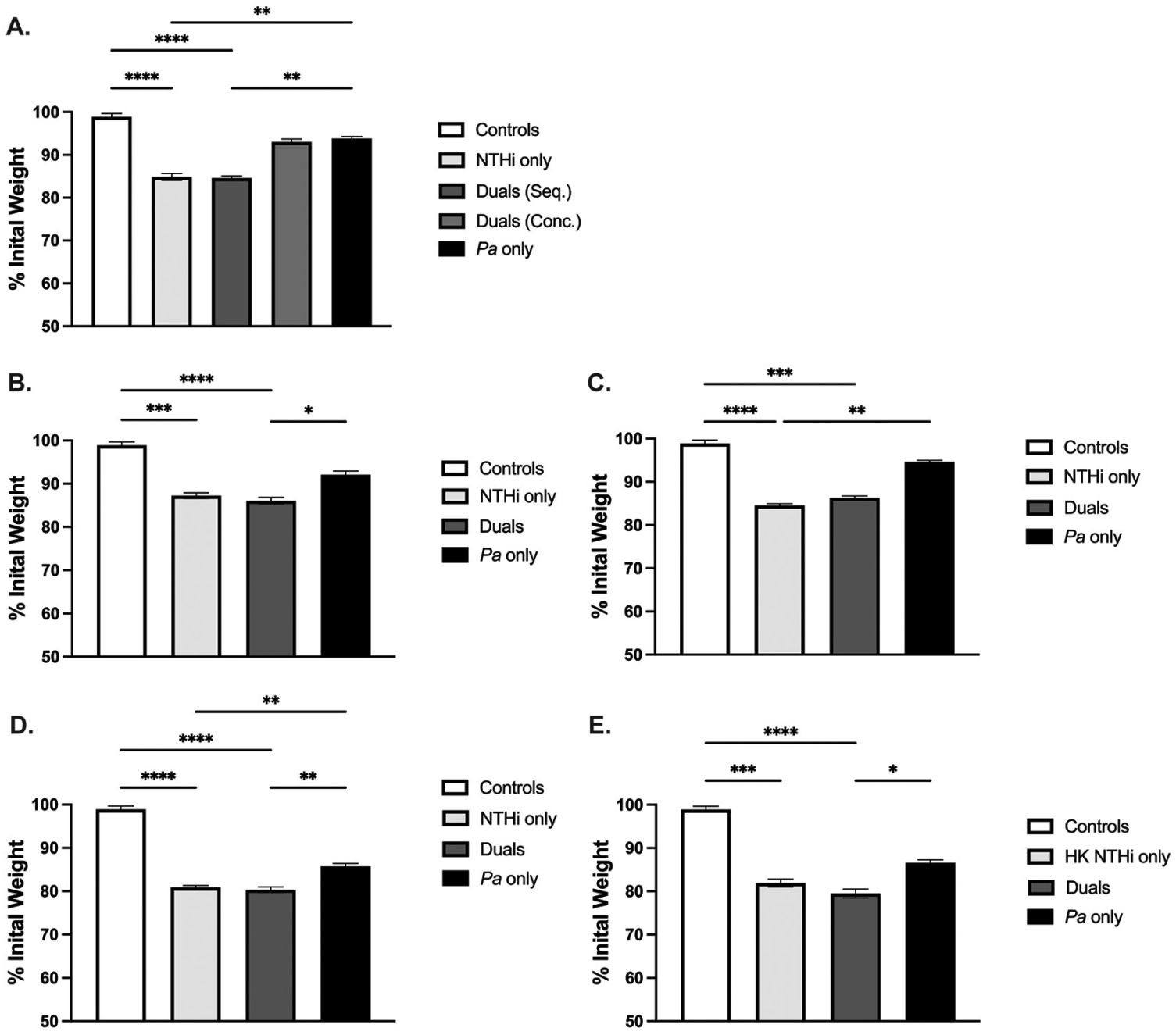

Fig. S2: Weight change following nontypeable *H. influenzae* and *P. aeruginosa* infection. Percentage of initial weight was calculated for all animal infections with weight change compared to uninfected controls. A) Weight change at 48 hours post-infection with NTHi HI-1r and mPA 08-31. B) Weight change at 72 hours post-infection with NTHi 86-028NPr and mPA 08-31. C) Weight change at 72 hours post-infection with NTHi HI-1r and *Pa* FRD1*mucA+.* D) Weight change at 72 hours post-infection with NTHi HI-1r and mPA 08-31. E) Weigh change at 72 hours post-infection with heat-killed NTHi HI-1r and mPA 08-31. (N = 10-15). Mean ± SEM. Kruskal-Wallis with Dunn's multiple comparison test, * P<0.05, ** P<0.01, *** P<0.001, **** P<0.0001.